J Comput Aided Mol Des (2006) 20:375–383
DOI 10.1007/s10822-006-9071-1

ORIGINAL PAPER

Mechanism of enhanced conversion of 1,2,3-trichloropropane by mutant haloalkane dehalogenase revealed by molecular modeling

Pavel Banáš · Michal Otyepka · Petr Jeřábek · Martin Petřek · Jiří Damborský

Received: 6 April 2006 / Accepted: 24 August 2006 / Published online: 3 October 2006

Abstract 1,2,3-Trichloropropane (TCP) is a highly toxic, recalcitrant byproduct of epichlorohydrin manufacture. Haloalkane dehalogenase (DhaA) from *Rhodococcus* sp. hydrolyses the carbon–halogen bond in various halogenated compounds including TCP, but with low efficiency (k_{cat}/K_m = 36 s^{-1} M^{-1}). A Cys-176Tyr-DhaA mutant with a threefold higher catalytic efficiency for TCP dehalogenation has been previously obtained by error-prone PCR. We have used molecular simulations and quantum mechanical calculations to elucidate the molecular mechanisms involved in the improved catalysis of the mutant, and enantioselectivity of DhaA toward TCP. The Cys176Tyr mutation modifies the protein access and export routes. Substitution of the Cys residue by the bulkier Tyr narrows the upper tunnel, making the second tunnel ''slot'' the preferred route. TCP can adopt two major orientations in the DhaA enzyme, in one of which the halide-stabilizing residue Asn41 forms a hydrogen bond with the terminal halogen atom of the TCP molecule, while in the other it bonds with the central halogen atom. The differences in these binding patterns explain the preferential formation of the (*R*)- over the (*S*)-enantiomer of 2,3-dichloropropane-1-ol in the reaction catalyzed by the enzyme.

Keywords Directed evolution · Enantioselectivity · Molecular dynamics · Nucleophilic substitution · Quantum mechanics · Tunnels

P. Banáš · M. Otyepka (✉)
Department of Physical Chemistry, Faculty of Science, Palacky University, tr. Svobody 26, 771 46 Olomouc, Czech Republic
e-mail: otyepka@aix.upol.cz

P. Jeřábek · J. Damborský (✉)
Loschmidt Laboratories, Faculty of Science, Masaryk University, Kamenice 5/A4, 625 00 Brno, Czech Republic
e-mail: jiri@chemi.muni.cz

M. Petřek
National Centre for Biomolecular Research, Faculty of Science, Masaryk University, Kamenice 5/A4, 625 00 Brno, Czech Republic

Introduction

Trihalogenated propanes are toxic synthetic hydrocarbons that have been released into the biosphere, generally as trace pollutants of agricultural products and industrial wastes. 1,2,3-Trichloropropane (TCP), formed as an undesirable side-product during the chemical production of epichlorohydrin and 1,2-dichloropropene, occurs as a water contaminant [1]. TCP is highly recalcitrant and resistant to biological degradation, even though thermodynamic calculations show that aerobic mineralization of TCP could provide sufficient energy to sustain microbial growth [2] and biological degradation of trihalogenated propanes can be catalyzed (albeit inefficiently) by haloalkane dehalogenase enzymes. Therefore, information on the biological degradation of TCP and the enzyme kinetics involved should be useful for assessing its likely durability, for developing possible ways to accelerate its elimination from different environments, and for exploring ways whereby TCP could be

recycled during the commercial production of epoxides [3].

The haloalkane dehalogenases (EC 3.8.1.5) are microbial enzymes that belong to the α/β-hydrolase superfamily [4–6] and catalyze the conversion of haloalkanes to the corresponding alcohols and a halide ion by a hydrolytic mechanism. The natural haloalkane dehalogenase that has the highest known activity toward TCP is the DhaA enzyme isolated from the soil bacterium *Rhodococcus rhodochrous* sp. NCIMB 13064. However, its catalytic efficiency is quite low (k_{cat}/K_m = 36 s^{-1} M^{-1}), preventing its use in practice [7]. DhaA (or RrDHL) consists of a main α/β-hydrolase fold domain and a helical cap domain [6]. The active site is an occluded cavity located between these two domains, and is connected to the surface by two export routes: an upper tunnel and a ''slot''. The catalytic triad Asp106-His272-Glu130 is positioned in the active site. The cleavage of the carbon–halogen bond involves two steps and proceeds via a covalent alkyl–enzyme intermediate. The carboxyl oxygen of the nucleophilic amino acid Asp106 attacks the carbon carrying a halogen substituent, cleaving off the halogen by an S_N2 substitution mechanism. Two primary halide-stabilizing amino acids, Asn41 and Trp107, are involved in the stabilization of the transition state and binding of the leaving halide ion. In the second reaction step, a catalytic water molecule activated by the His272 hydrolyzes the covalent alkyl–enzyme intermediate by an Ad_N mechanism. The corresponding primary alcohol, halide ion and proton are the products created during the reaction [8].

A directed evolution method called error-prone PCR has been used by Bosma et al. [7] to generate DhaA mutants, including the Cys176Tyr (M1-DhaA) mutant, which showed three times higher catalytic efficiency toward TCP (k_{cat}/K_m = 100 s^{-1} M^{-1}) compared to the wild-type enzyme (WT-DhaA). Molecular modeling was then used to obtain information on the effect of mutations on catalytic properties. Molecular docking analysis predicted three different orientations of TCP in the active site that have been denoted binding modes BM1, BM2 and BM3 (Fig. 1), and possible dehalogenation mechanisms of the C_α/C_β carbon atoms were discussed [7].

Here we present a thorough analysis of the wild-type and mutant enzymes using molecular dynamic (MD) simulations and quantum mechanical (QM) calculations. The study provides insight into the molecular mechanism underlying the enhanced catalytic activity of M1-DhaA and the enantioselectivity of the DhaA enzyme.

Methodology

In silico mutagenesis

The starting geometry of M1-DhaA was generated from the crystal structure of free wild-type DhaA (WT-DhaA; PDB entry 1CQV). The structures of side-chains of mutated residues were modeled using the program Deep View [9]. The Cys176Tyr mutation resulted in two possible conformations of the Tyr176 side-chain that differed in torsions N–C_α–C_β–C_γ and C_α–C_β–C_γ–C_δ. A structurally and energetically feasible rotamer of Tyr176 was determined by two 700-ps MD simulations of DhaA, starting with Tyr176 in two different conformations.

MD simulations

Starting geometries for MD simulations were prepared from crystal structures after necessary modifications. Hydrogen atoms were added using the program WHATIF [10], and His272 was N_δ-protonated in accordance with the reaction mechanism. The system was neutralized by adding 18 Na^+ counter ions using GRID [11] and immersed in a rectangular water box with a 10-Å wide layer of water molecules. The active site was solvated in accordance with previous study [12] demonstrating only small changes in active site volume and capacity to accept only six water molecules. The molecular docking placed the substrate to the same positions as occupied by four active site waters, which were subsequently removed leaving on catalytic and stabilizing water in their crystallographic positions. The protein–solvent system was optimized prior to the simulation as follows. Minimization of the enzyme hydrogens was followed by minimization of the substrate, counter ions and crystal waters. Subsequently, the protein was frozen and solvent molecules with counter ions were allowed to move during a 10-ps MD run. The side-chains were allowed to relax in several minimization runs with decreasing force constants applied to the backbone atoms. After full relaxation, the system was slowly heated to 300 K over 100 ps using a 2-fs time step and NpT conditions. All the simulations were calculated under periodic boundary conditions in the NpT ensemble (300 K, 1 atm) with 2 fs time steps. The particle-mesh Ewald method was used to calculate electrostatic interactions and a 9.0-Å cutoff was applied for Lennard–Jones interactions. The SHAKE algorithm was applied to fix all bonds containing hydrogen atoms. The SANDER module of AMBER 6.0 with the Cornell et al. force field [13] was used for all simulations. Partial atomic

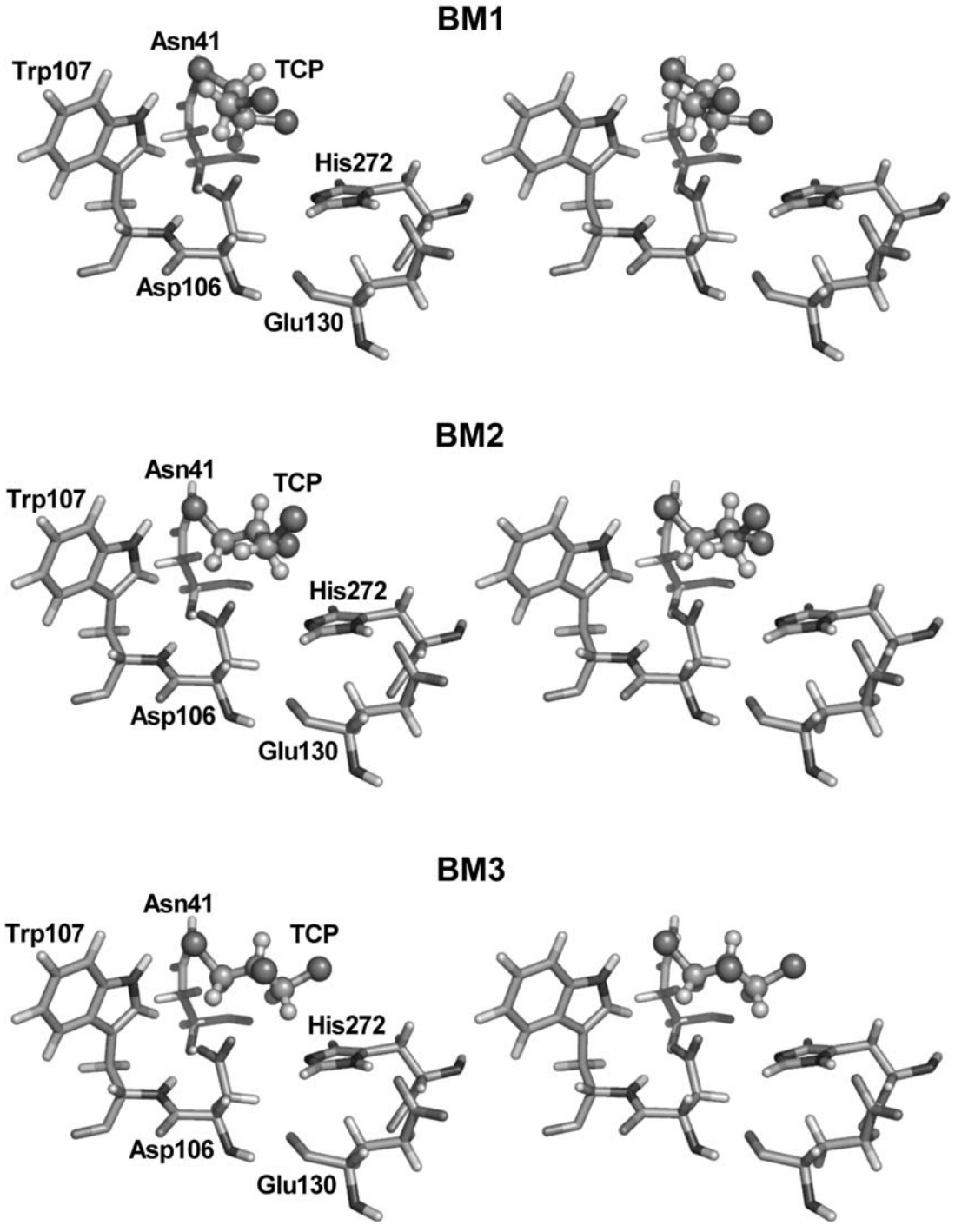

Fig. 1 The three binding modes of TCP (BM1, BM2 and BM3) in the active site of DhaA predicted by molecular docking [7]. The corresponding reaction products from the three binding modes are 1,3-dichloropropane-2-ol, (*S*)-2,3-dichloropropane-1-ol and (*R*)-2,3-dichloropropane-1-ol, respectively. The catalytic triad Asp106, His272, Glu130 and the primary halide-stabilizing residues Trp107 and Asn41 are shown in *stick form*

charges for TCP and esterificated Asp106 were determined using the restrained electrostatic potential procedure [14]. The required ab initio calculations were carried out using the Gaussian98 program [15] at the HF/6–31G(d) level of theory. MD simulations of the following structures were carried out: (a) enzyme–substrate complexes of WT-DhaA and M1-DhaA with TCP in BM1, BM2 and BM3 (six 1 ns simulations) and

(b) the alkyl–enzyme intermediates of WT-DhaA and M1-DhaA with esterificated Asp106 corresponding to TCP in BM2 and BM3 (four 2 ns simulations). Results of the MD simulations were analyzed using the Carnal and Ptraj modules of the AMBER 6.0 package [16]. Decomposition analysis was performed using the Anal module of the AMBER 6.0 package. The stability of the simulations was verified by comparing radii of gyration, root-mean-square deviations and B-factors with previous values obtained from simulation with free DhaA [12]. The occupation of each binding mode during the simulations was quantified by calculating Mahalanobis distances in configuration space [17] between near attack conformation (NAC) [18] and the actual orientation of TCP.

Semi-empirical QM calculations

The S_N2 reaction step was studied by semi-empirical calculations using the AM1 Hamiltonian [19] and the following segment of the active site: Asn41, Asp106, Trp107, Glu130, Ile132, Trp141, Phe149, Phe168, Val172, Cys/Tyr176, Phe205, Pro206, Phe209, Val245, Leu246, His272 and Tyr/Phe273. Two water molecules from the active site were also included in the calculations. Average structures of TCP obtained from the MD simulations of enzyme–substrate complexes in various conformations were taken as the starting orientations of TCP. Both Cl–C–C–Cl torsions appeared in *gauche* and/or *trans* conformations during the MD simulations, therefore the four averaged conformations of TCP were used for the QM calculations. In total, 16 calculations were performed with permutations of two protein variants (WT-DhaA and M1-DhaA) and two binding modes of TCP (BM2 and BM3) in four torsion conformations (*gauche–gauche*, *gauche–trans*, *trans–gauche* and *trans–trans*). The reaction path was modeled by shortening the distance between oxygen $O_{\delta 1}$ of the nucleophilic Asp106 of DhaA and the attacked carbon atom of TCP. The geometry was fully optimized, except for the driven coordinate after each 0.05 Å-long driving step. Heavy atoms of the backbone and oxygen from the catalytic water were fixed to constrain the active site structure. The TRITON program [20, 21] was used to prepare input and analyze output files. The semi-empirical QM package MOPAC2002 [22] with the external subroutine DRIVER [23] was used for mapping the reaction pathway. All MOPAC calculations were carried out using the AM1 Hamiltonian and the Broyden–Fletcher–Goldfarb–Shanno, quasi-Newton algorithm geometry optimization algorithm. MOZYME was used to speed up SCF calculations.

Results

Dynamics of export routes

The energy decomposition method was used for partitioning electrostatic and van der Waals interaction energy contributions to the interactions between the mutated residue (Cys/Tyr176) and other residues in WT-DhaA and M1-DhaA. Mutation Cys176Tyr generally has a minor influence on the interaction energies of Cys/Tyr176 with most protein residues. However, the mutation increased attraction between Cys/Tyr176 and Phe144, and decreased attraction between Cys/Tyr176 and Leu173 or Lys175 (Table 1). Phe144, Leu173 and Lys175 residues are located near Cys/Tyr176 and collectively form the opening of the so-called upper tunnel [12]. This observation prompted us to investigate the structure and dynamics of this tunnel in greater detail.

The diameter of the upper tunnel was calculated for all enzyme–substrate and alkyl–enzyme intermediate simulations (Table 2) using the program CAVER [24]. This program monitors changes in tunnel radius during MD simulations and identifies preferred export routes. The mean radius of the upper tunnel in WT-DhaA is 1.31 ± 0.01 Å (averaged through all WT-DhaA simulations), while in M1-DhaA it is substantially smaller; 0.61 ± 0.01 Å (averaged through all M1-DhaA simulations). The mean radius of the second tunnel of DhaA, called the slot, is 0.80 ± 0.01 Å in both WT-DhaA and M1-DhaA simulations (Fig. 2). The program CAVER assigned the upper tunnel as the preferred export route in WT-DhaA, while the slot was favored in M1-DhaA. This observation was consistent with expectations since residue 176 points toward the entrance tunnel (Fig. 2). The other main differences noted between WT-DhaA and M1-DhaA were in the dynamics of water molecules in the active site of the alkyl–enzyme intermediate. Three water molecules located near the entrance to the slot are exchangeable with water molecules from the bulk solvent. Traffic of water molecules between the slot, active site and upper tunnel was observed in the simulation of WT-DhaA

Table 1 Interaction energies (in kJ mol^{-1}) between the mutated residue and other residues in the protein, showing the largest differences between WT-DhaA and M1-DhaA

Mutated residue	Interacting residue	DhaA-WT	DhaA-M1
Cys/Tyr176	Phe144	–0.8	–6.7
	Leu173	–12.6	–7.5
	Lys175	–128.4	–118.0

Table 2 Mean radii (in Å) of the upper tunnel calculated from MD simulations (using the program CAVER)

Protein	Enzyme–substrate complex			Alkyl–enzyme intermediate	
	BM1	BM2	BM3	BM2	BM3
WT-DhaA	1.24 ± 0.06	1.12 ± 0.05	1.61 ± 0.05	1.14 ± 0.03	1.43 ± 0.02
M1-DhaA	0.63 ± 0.04	0.70 ± 0.05	0.54 ± 0.03	0.54 ± 0.02	0.62 ± 0.02

(TCP in BM3). One water molecule entered the active site via the slot (at 135 ps) and the same molecule left through the upper tunnel (at 1,510 ps). Analogous water traffic has been found in previous simulations of free WT-DhaA [12], but not the movement of water molecules through the upper tunnel of M1-DhaA.

TCP dynamics in the enzyme active site

Six MD simulations were conducted for WT-DhaA and M1-DhaA complexes with TCP bound in three different binding modes. The concept of NAC, i.e., a configuration suitable for enzymatic reaction [18], was used to characterize TCP behavior in the active site. We used the Mahalanobis distance as a generalized statistical distance in configuration space for quantitative analysis of NACs. The NAC was defined by three parameters: (a) the distance between the nucleophilic oxygen of Asp106 and the attacked carbon of TCP, (b) the angle between the nucleophilic oxygen of Asp106, the attacked carbon and the leaving chlorine of TCP, and (c) the sum of distances between the leaving chlorine and side-chain nitrogens of the halide-stabilizing residues Asn41 and Trp107. The distance between the NAC of each binding mode and the actual position of TCP in the MD trajectory was used to monitor changes in binding mode during the simulations. Rearrangement of TCP from BM1 to BM2 was observed in both simulations starting from BM1, and a switch from BM1 to BM2 occurred during the first 500 ps of the simulation (Fig. 3), while BM2 and BM3 were stable in all simulations (Table 3). The populations of NACs calculated for WT-DhaA and M1-DhaA were very similar, indicating that the Cys176Tyr mutation does not affect the reactivity of the respective enzyme–substrate complexes.

The Cl_l–C_a–C–Cl torsion (torsion ψ) with the attacked carbon (C_a) and leaving chlorine (Cl_l) adopted *gauche* conformation during the simulations, while the other torsion (Cl–C–C–Cl torsion ϕ) varied between *trans* and *gauche* conformations (Table 4). The torsions ψ and ϕ of BM2 appear in *gauche*(-) and *gauche*(+) conformations, respectively, while BM3 torsions ψ and ϕ prefer *gauche*(+) and *gauche*(-) conformations, respectively (Fig. 1). The distance between the Asn41 amidic nitrogen $N_{\delta 2}$ (which stabilizes the leaving chlorine) and TCP's central chlorine is influenced by the sign of the *gauche* ψ torsion. This distance equals 4.5 ± 0.8 Å in BM2 [ψ = *gauche*(-)] and 6.6 ± 0.4 Å in BM3 [ψ = *gauche*(+)]. The difference between binding modes BM2 and BM3 may be related to the reactivity of the respective complexes and explain the enantioselectivity of DhaA enzymes (see next paragraph).

Reactivity of TCP in the enzyme active site

S_N2 dehalogenation of TCP in the active site of DhaA was studied using the AM1 method. The enzyme–TCP complexes obtained from the docking were used as starting geometries. All calculations that started from BM1 yielded high activation barriers (Table 5). The $C_{\alpha 1}$ carbon atom was identified as the most favored center for the S_N2 attack of TCP in BM2, leading to the corresponding reaction product (*S*)-2,3-dichloropropane-1-ol. On the other hand, the $C_{\alpha 2}$ carbon atom is the likeliest electrophilic site for dehalogenation of TCP in BM3, yielding (*R*)-2,3-dichloropropane-1-ol. The dehalogenation of other carbons is not possible due to high activation barriers (E^a) and lack of halide stabilization, with unfavorable reaction enthalpy (ΔH).

The time-averaged structures from MD simulations were subsequently used for AM1 calculations. Four different TCP conformations observed in the simulations were used as the starting geometries. The mean activation barriers and reaction enthalpies significantly differed between BM2 and BM3, but not between WT-DhaA and M1-DhaA (Table 6). Activation barriers for the dehalogenation reaction starting from BM2 were significantly higher than for BM3, due to the absence of a hydrogen bond between the halide-stabilizing residue Asn41 and the leaving halogen (Fig. 4). A correlation (with a Pearson correlation coefficient of 0.81) was observed between the activation barrier E^a and the stabilizing effect of Asn41, reflecting the distance between Asn41 $N_{\delta 2}$ and the leaving chlorine in the transition state.

Discussion

The side-chain of Cys176 forms a bottleneck in the upper tunnel of DhaA. The differences in the

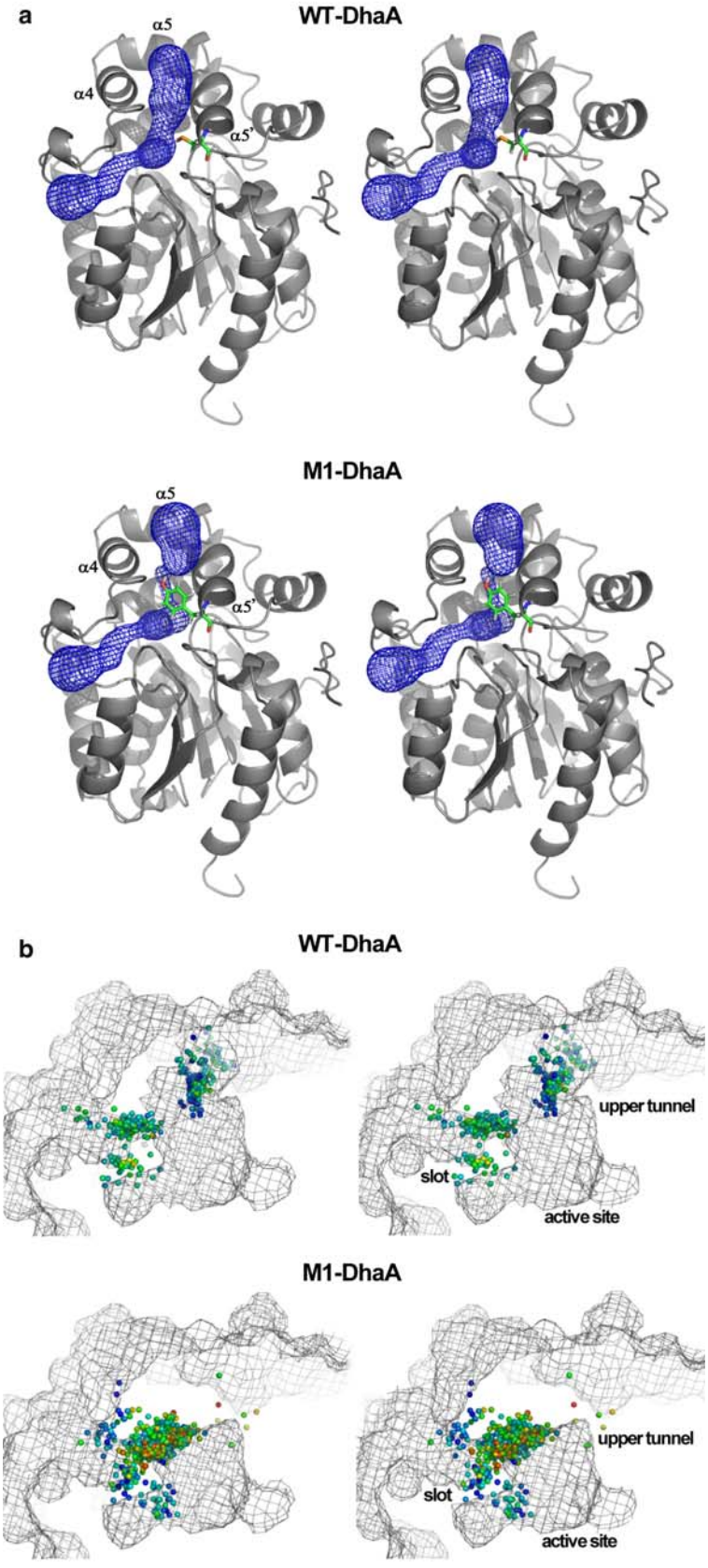

Fig. 2 **a** Visualization of residue 176 in WT-DhaA (Cys) and M1-DhaA (Tyr). The upper tunnel is the most favorable path in WT-DhaA, while the slot is the more easily accessible path in the mutant. The side-chain of Tyr points toward the upper tunnel located between helixes α4, α5′, and α5 of the cap domain [12], leaving the slot as the only export route from the active site to the protein's exterior. Proteins are represented in *cartoon*, tunnels in *mesh surface* and the side-chain of residue 176 in *stick formats*. **b** Population of the most preferable paths in snapshot structures from MD trajectories of WT-DhaA and M1-DhaA. Access tunnels are represented by *mesh surface*. *Balls* represent the gorges of the most preferable access paths colored by the radii of the gorges: the *red part* of the spectrum denotes narrow gorges and *blue spectrum* wider gorges. Both the upper tunnel and slot are populated in WT-DhaA, while the slot is the sole preferred path in M1-DhaA

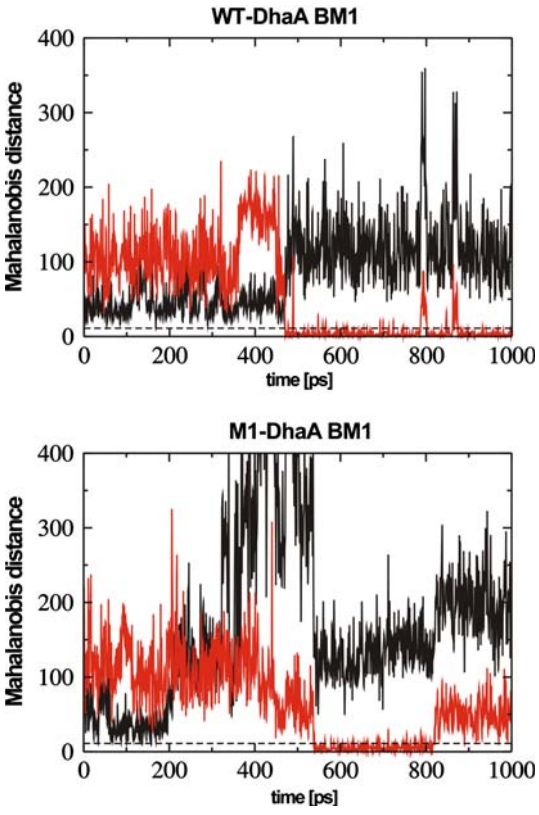

Fig. 3 The Mahalanobis distance in configuration space indicating the distance between the actual orientation of TCP in MD simulations and the NAC conformations of BM1 (*black line*) and BM2 (*red line*). The TCP rearranges from BM1 to BM2 within 480 ps in the WT-DhaA simulation and remains bound in BM2, while it rearranges from BM1 to BM2 within 380 ps in the M1-DhaA simulation and remains bound in BM2 between 530 and 810 ps. The Mahalanobis distance value fluctuating under the value 11 (0.01 χ^2-quantile, with three degrees of freedom, *dashed line*) corresponds to TCP bound to the correspondent binding mode

Table 3 The occupation of NAC (in %) for the starting binding modes BM2 and BM3

	BM2	BM3
WT-DhaA	92.2	97.9
M1-DhaA	89.8	95.2

Table 4 The population of four TCP conformations (in %) represented by ψ and ϕ torsions in enzyme–substrate complexes during MD simulations

Torsion ψ	Torsion ϕ	WT/ BM2	M1/ BM2	WT/ BM3	M1/ BM3
Gauche	*Gauche*	73.7	71.5	34.8	49.8
Gauche	*Trans*	20.4	19.0	63.2	49.1
Trans	*Gauche*	5.7	9.5	1.9	0.6
Trans	*Trans*	0.2	0.0	0.1	0.5

Table 5 Activation energies, E^a, and reaction enthalpies ΔH (in kJ mol^{-1}) of the S_N2 dehalogenation reaction calculated for binding modes BM1, BM2 and BM3 of TCP in WT-DhaA predicted by molecular docking

Attacked atom	BM1 E^a	ΔH	BM2 E^a	ΔH	BM3 E^a	ΔH
$C_{\alpha 1}$	349.8	–2.5	89.5	–51.9	149.8	–19.2
C_β	398.3	–6.3	374.9	–9.2	348.5	21.3
$C_{\alpha 2}$	133.1	–64.9	178.2	28.0	100.8	–58.6

Table 6 Activation energies, E^a, and reaction enthalpies ΔH (in kJ mol^{-1}) of the S_N2 dehalogenation reaction started from time-averaged MD structures

Enzyme type	BM2 E^a	ΔH	BM3 E^a	ΔH
WT-DhaA	117.6	–22.2	108.8	–49.0
M1–DhaA	115.5	–18.8	100.4	–61.9

The energies were calculated as weighted mean values of energies corresponding to four different TCP conformations with respect to the population of the TCP conformations obtained through MD simulations (see Table 4)

WT-DhaA and M1-DhaA MD simulations show that the radius of this tunnel is significantly narrowed by the Cys176Tyr mutation and, consequently, another opening to the active site, called the slot, becomes the preferred access or export route in M1-DhaA. The exchange of ligands between the bulk solvent and the enzyme's active site appears to be significantly affected by this change. Previous D_2O solvent kinetic isotope effect experiments, in which the dehalogenation of TCP by WT-DhaA was explored [25], revealed that the rate-determining step lies before cleavage of the alkyl–enzyme intermediate, i.e., substrate-binding or carbon–halogen bond cleavage is the rate-limiting step. QM calculations of carbon–halogen bond cleavage (the S_N2 step) did not provide any indications that the activation barriers differed between WT-DhaA and M1-DhaA. Thus, the Cys176Tyr mutation probably improves the efficiency of the enzyme by increasing the rate of substrate binding. The underlining mechanism could be existence of energetically favorable binding site located adjacent to the face of the catalytic histidine near the entry to the main tunnel. This binding site was observed for the crystal structure of LinB (a haloalkane dehalogenase involved in the degradation of γ-hexachlorocyclohexane by *Sphingobium japonicum* UT26) in its complex with the substrates 1,2-dichloroethane and 1,2-dichloropropane, as well as with the product molecule 1-butanol [26]. Binding of various ligands to the same site can be

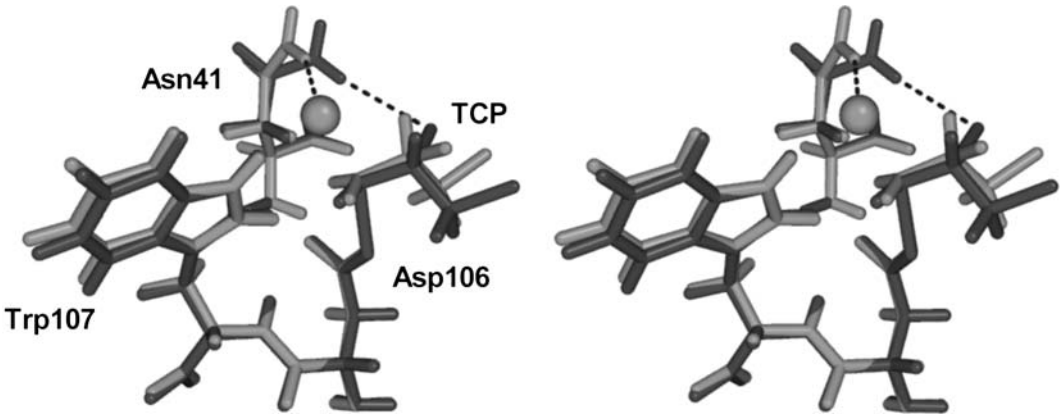

Fig. 4 Superposition of transition state structures of the wild-type protein and TCP in BM2 (*black*) and BM3 (*gray*) obtained from QM calculations. Only the nucleophile Asp106 and two primary halide-stabilizing residues, Asn41 and Trp107, are shown (in *stick form*) for clarity. The residue Asn41 forms a hydrogen bond (*dashed line*) with the central halogen in BM2, and with the leaving halogen (*ball*) in BM3, thereby altering the thermodynamic parameters of the S_N2 reaction. The same hydrogen bonds were observed in 2 ns MD simulations

found also in the structures of other protein–ligand complexes [27, 28] including the complex of LinB with dehalogenation product of TCP (PDB ID 2BFN). Ligands passing through the main tunnel of LinB and DhaA must come into contact with this site. Redirecting ligands from the main tunnel to the slot prevents their binding to this local energetic minimum. We note that Cys176 in DhaA is analogous to Leu177 of LinB, which was substituted by all possible amino acids via site-directed mutagenesis in a study by Chaloupkova et al. [29]. Resulting protein variants with modified tunnel radii showed significant differences in their catalytic properties. We predict that catalytic rate of TCP conversion by DhaA mutant can be further improved by geometric optimization of the slot. Experimental validation of this proposal by using targeted directed evolution experiments is ongoing in our laboratory.

Computer simulations enable real-time monitoring of the spatial distribution of a ligand molecule inside an enzyme's active site. The TCP molecule bound in BM1 was unstable in all MD simulations and switched from BM1 to BM2 within the first 500 ps of simulation. Furthermore, QM calculations indicated that the activation energy of the S_N2 reaction starting from BM1 is very high. Thus, the probability of chemical reaction occurring from BM1 is close to zero under normal conditions. The instability of BM1 and the high activation barrier explains why the secondary alcohol (1,3-dichloropropane-2-ol) has never been observed as the dehalogenation product of TCP [7]. In contrast, the high stability of the enzyme–substrate complexes, the low activation energy and favorable reaction enthalpy of the S_N2 reaction step during the MD simulations starting with TCP in BM2 and BM3 confirm that carbon–halogen cleavage can proceed effectively from both BM2 and BM3 modes. The reaction product corresponding to BM2 is (*S*)-2,3-dichloropropane-1-ol, while (*R*)-2,3-dichloropropane-1-ol is the reaction product of TCP starting from BM3. The S_N2 reaction step has higher activation energy and less favorable enthalpy when TCP is bound in BM2 compared to BM3, irrespective of the protein variant. The less favorable reaction conditions for BM2 are due to weaker stabilization of the leaving chlorine by Asn41, which forms a competitive interaction with the middle chlorine of TCP. The difference in the reactivities of the substrates starting from BM2 and BM3 explain the experimentally observed preferential formation of (*R*)-2,3-dichloropropane-1-ol over (*S*)-2,3-dichloropropane-1-ol by DhaA-WT [7].

Acknowledgments We thank Dr Tjibe Bosma (Groningen, the Netherlands) for valuable discussions on the interpretation of kinetic characterizations of mutant dehalogenases. We acknowledge financial support from the Czech Ministry of Education (MO, grants MSM6198959216, LC512; JD, grant MSM0021622412). The research of JD is supported by an EMBO/HMMI grant within the Young Investigator Program. We thank Dr J. Blackwell (UK) for linguistic revisions.

References

1. Tesoriero AJ, Loffler FE, Liebscher H (2001) Environ Sci Technol 35:455–461
2. Dolfing J, Janssen DB (1994) Biodegradation 5:21–28
3. Swanson PE (1999) Curr Opin Biotechnol 10:365–369
4. Verschueren KHG, Seljee F, Rozeboom HJ, Kalk KH, Dijkstra BW (1993) Nature 363:693–698

5. Ollis DL, Cheah E, Cygler M, Dijkstra B, Frolow F, Franken SM, Harel M, Remington SJ, Silman I, Schrag J, Sussman JL, Verschueren KHG, Goldman A (1992) Protein Eng 5:197–211
6. Newman J, Peat TS, Richard R, Kan L, Swanson PE, Affholter JA, Holmes IH, Schindler JF, Unkefer CJ, Terwilliger TC (1999) Biochemistry 38:16105–16114
7. Bosma T, Damborsky J, Stucki G, Janssen DB (2002) Appl Environ Microbiol 68:3582–3587
8. Janssen DB (2004) Curr Opin Chem Biol 8:150–159
9. Guex N, Peitsch MC (1997) Electrophoresis 18:2714–2723
10. Vriend G (1990) J Mol Graph 8:52–56
11. Goodford PJ (1985) J Med Chem 28:849–857
12. Otyepka M, Damborsky J (2002) Protein Sci 11:1206–1217
13. Cornell WD, Cieplak P, Bayly CI, Gould IR, Merz KM, Ferguson DM, Spellmeyer DC, Fox T, Caldwell JW, Kollman PA (1995) J Am Chem Sci 117:5179–5197
14. Cornell WD, Cieplak P, Bayly CI, Kollman PA (1993) J Am Chem Soc 115:9620–9631
15. Frisch MJ, Frisch A, Foresman JB (1998) Gaussian 98. Gaussian Inc., Pittsburgh
16. Case DA, Pearlman DA, Caldwell JW, Cheatham TE III, Ross WS, Simmerling CL, Darden TA, Merz KM, Stanton RV, Cheng AL, Vincent JJ, Crowley M, Tsui V, Radmer RJ, Duan Y, Pitera J, Seibel GL, Singh UC, Weiner PK, Kollman PA (1999) V. AMBER 6.0. University of California, San Francisco
17. Mahalanobis PC (1936) Proc Natl Inst Sci India 2:49–55
18. Lightstone FC, Zheng YJ, Bruice TC (1998) J Am Chem Soc 120:5611–5621
19. Dewar MJS, Zoebisch EG, Healy EF, Stewart JJP (1985) J Am Chem Soc 107:3902–3909
20. Damborsky J, Prokop M, Koca J (2001) Trends Biochem Sci 26:71–73
21. Prokop M, Damborsky J, Koca J (2000) Bioinformatics 16:845–846
22. Stewart JJP (1990) J Comput Aided Mol Des 4:1–45
23. Cernohorsky M, Kuty M, Koca J (1996) Comput Chem 21:35–44
24. Petrek M, Otyepka M, Banas P, Kosinova P, Koca J, Damborsky J (2006) BMC Bioinformatics 7:316
25. Bosma T, Pikkemaat MG, Kingma J, Dijk J, Janssen DB (2003) Biochemistry 42:8047–8053
26. Oakley A, Prokop Z, Bohac M, Kmunicek J, Jedlicka T, Monincova M, Kuta-Smatanova I, Nagata Y, Damborsky J, Wilce MCJ (2002) Biochemistry 41:4847–4855
27. Marek M, Vevodova J, Kuta-Smatanova I, Nagata Y, Swensson LA, Newman J, Takagi M, Damborsky J (2000) Biochemistry 39:14082–14086
28. Streltsov VA, Prokop Z, Damborsky J, Nagata Y, Oakley A, Wilce MCJ (2003) Biochemistry 42:10104–10112
29. Chaloupkova R, Sykorova J, Prokop Z, Jesenska A, Monincova M, Pavlova M, Tsuda M, Nagata Y, Damborsky J (2003) J Biol Chem 278:52622–52628